

Multi-focus Image Fusion with Sparse Feature Based Pulse Coupled Neural Network

Yongxin Zhang^{1,2}, Li Chen^{*1}, Zhihua Zhao¹, Jian Jia³

¹ School of Information Science and Technology, Northwest University, Xi'an 710127, Shaanxi, China

² Luoyang Normal University, Luoyang 471022, He'nan, China

³ Department of Mathematics, Northwest University, Xi'an 710127, Shaanxi, China

*Corresponding author, e-mail: tabo126@126.com

Abstract

In order to better extract the focused regions and effectively improve the quality of the fused image, a novel multi-focus image fusion scheme with sparse feature based pulse coupled neural network (PCNN) is proposed. The registered source images are decomposed into principal matrices and sparse matrices by robust principal component analysis (RPCA). The salient features of the sparse matrices construct the sparse feature space of the source images. The sparse features are used to motivate the PCNN neurons. The focused regions of the source images are detected by the output of the PCNN and integrated to construct the final fused image. Experimental results show that the proposed scheme works better in extracting the focused regions and improving the fusion quality compared to the other existing fusion methods in both spatial and transform domain.

Keywords: image fusion, robust principal component analysis, pulse-coupled neural network, sparse feature, firing times

1. Introduction

Multi-focus image fusion is a process that different images with different settings are integrated to produce a new image contains all relevant objects in focus, which is very useful for human or machine perception [1]. In general, image fusion methods can be categorized into two groups: spatial domain fusion and transform domain fusion [2]. The spatial domain fusion methods are easy to implement and have low computational complexity, but the spatial domain methods may produce blocking artifacts and compromise the quality of the final fused image. Different from the spatial domain fusion, the transform domain fusion methods can get improved contrast, better signal-to-noise ratio and better fusion quality [3], but the transform domain fusion methods are time/space-consuming to implement.

Pulse coupled neural network (PCNN) is a novel visual cortex-inspired neural network characterized by the global coupling and pulse synchronization of neurons, which was developed by Eckhorn et al. [4] in the experimental observation of synchronization bursts in cat and monkey visual cortex in 1990. Broussard et al. [5] have firstly applied PCNN in image fusion for object detection and Johnson et al. [6] have pointed out the great potential of PCNN in the field of data fusion in the same year. It has been observed that PCNN based image fusion methods outperform the conventional methods [7]. So far, many multi-focus image fusion methods based on PCNN have been proposed [8]-[12]. However, most of them suffer from various problems. Miao et al. [8] have proposed a fusion method using the sharpness of a small neighborhood of each pixel as the linking strength of PCNN. It works better in preserving edge and texture information, but suffers from contrast reduction. Huang et al. [9] have proposed a fast fusion method based on energy of the image laplacian (EOL) motivated PCNN in spatial domain. It produces the blocking artifacts in fused image while improves the fusion speed. Qu et al. [10] have developed a fusion method based on spatial frequency (SF) motivated PCNN in nonsubsampled contourlet transform (NSCT) domain. It works well for multi-focus image and visible/infrared image, but the absence of directional information in SF and the use of the same fusion rule for all the sub-bands lead to the contrast reduction and the loss of image details. Wang et al. [11] have proposed a fusion scheme based on dual-channel PCNN. This scheme motivates the dual-channel PCNN by using the EOL of the pixel's neighborhood and achieves better fusion result. It improves the quality of the fused image, but consumes more time. Geng et al. [12] have developed the fusion method based on PCNN in shearlet domain. It improves

the quality of the fused image, but the absence of shift invariant in shearlet transformation leads to the unwanted image degradations.

Different from the fusion methods mentioned above, in this paper, a new method of multi-focus image fusion with sparse feature based PCNN is proposed. Robust principal component analysis (RPCA) [13] is an important method of low-rank matrix recovery, which decomposes an image into a low-rank matrix which corresponds to the background, and a sparse one which links to salient objects [14]. Wan et al. [15] have investigated the potential application of RPCA in the multi-focus image fusion and achieved a consistently good fusion result, but their method requires longer computational time. Different from Wan's method, the main contribution of this paper is that the sparse features of the source images are used to motivate the PCNN neurons for image fusion. The sparse matrices of the source images are obtained by using RPCA decomposition. The sparse feature computed from the sparse matrices are used to motivate the PCNN neurons. The focused regions are detected by comparing the firing times of the PCNN neurons. The proposed method can efficiently extract the focused regions details from the source images and improve the visual quality of the fused image.

The rest of the paper is organized as follows. In section 2, the basic idea of RPCA and PCNN will be briefly described, followed by the new method with RPCA and PCNN for image fusion in section 3. In section 4, extensive simulations are performed to evaluate the performance of the proposed method. In addition, several experimental results are presented and discussed. Finally, concluding remarks are drawn in section 5.

2. Related Work

2.1. Robust Principal Component Analysis

RPCA is an effective way to recover both low-rank and sparse components exactly from high dimensional data by solving the principal component pursuit [13]. In which, an input data matrix $D \in \mathbb{R}^{M \times N}$ is subject to low-rank property. In order to recover the low-rank structure of D , D can be decomposed as:

$$D = A + E, \quad \text{rank}(A) = \min(M, N) \quad (1)$$

where matrix A is a principal matrix, and E is a sparse matrix. It is obvious that this problem is difficult to solve. Recently, Wright et al [16] have demonstrated that when the sparse matrix E is sufficiently sparse (relative to the rank of A), one can accurately recover the principal matrix A from D by solving the following convex optimization problem [17]:

$$\min_{A, E} \|A\|_* + \lambda \|E\|_1 \quad \text{s.t.} \quad A + E = D \quad (2)$$

where $\|\cdot\|_*$ denotes the nuclear norm of matrix A , λ is a positive weighting parameter, and $\|\cdot\|_1$ denotes the l_1 norm of the matrix E .

Candes et al. [13] have extended the RPCA to the background modelling from surveillance video. They correctly identified the moving pedestrians in the foreground by using the sparse component of surveillance video. The sparse matrix E represents the salient feature of the foreground object effectively. As is known, the salient objects in the foreground are very important for multi-focus image fusion. Motivated by Candes's idea, this paper tries to extract the sparse feature of the source images by using RPCA decomposition. Figure 1 (a) shows the multi-focus source images 'Book'. Figure 1 (b) and 1 (c) show the corresponding images of the principal matrix A and sparse matrix E , respectively. It is obvious that the salient features of sparse matrix E agree well with the local features of the focused objects in the source images. In this paper, the sparse features computed from the sparse matrix E are used to motivate the PCNN neurons, which will be introduced in the following subsection.

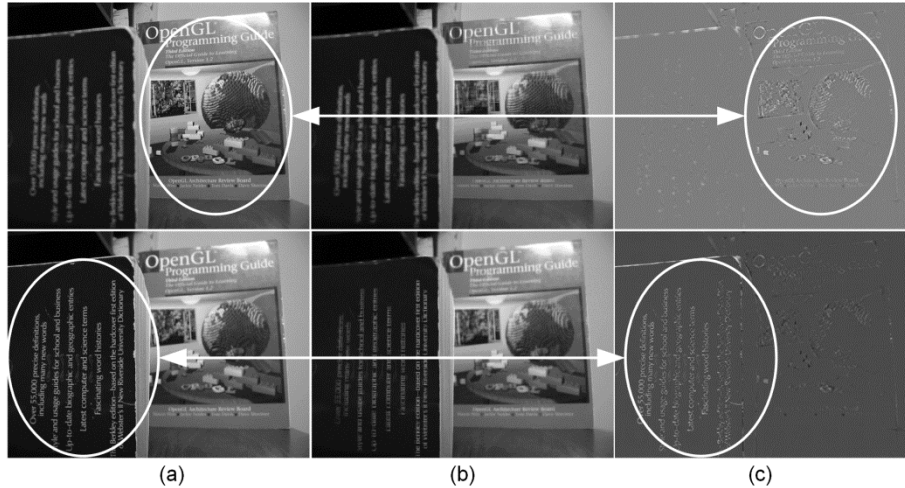


Figure 1. Decomposition of multi-focus images 'Book' using RPCA: (a) Source images D ; (b) Principal matrix A ; (c) Sparse matrix E

2.2. Pulse Coupled Neural Network

PCNN is a feedback network and belongs to the third generation artificial neural network. In image processing, PCNN is a single layered, two-dimensional, laterally connected with image pixels each other. Each PCNN neuron consists of three parts: the receptive field, modulation field and pulse generator. The PCNN neuron's specific structure is shown in Figure 2. The neuron can be described as[7]:

$$\begin{cases} F_{ij}(n) = e^{-\alpha_F} F_{ij}(n-1) + S_{ij} + V_F \sum_{kl} M_{ijkl} Y_{kl}(n-1) \\ L_{ij}(n) = e^{-\alpha_L} L_{ij}(n-1) + V_L \sum_{kl} W_{ijkl} Y_{kl}(n-1) \\ U_{ij}(n) = F_{ij}(n)[1 + \beta L_{ij}(n)] \\ Y_{ij}(n) = \begin{cases} 1 & U_{ij}(n) > \theta_{ij}(n) \\ 0 & \text{otherwise} \end{cases} \\ \theta_{ij}(n) = e^{-\alpha_\theta} \theta_{ij}(n-1) + V_\theta Y_{ij}(n-1) \end{cases} \quad (3)$$

Where the indexes i and j refer to the pixel location in the image, k and l refer to the dislocation in a symmetric neighborhood around the one pixel. n denotes the current iteration and S_{ij} denotes the input stimulus such as the normalized gray level of image pixels. α_F , α_L and α_θ are the decay constants of the PCNN neuron. V_F , V_L and V_θ are the magnitude scaling terms. The constant β is the linking strength. F_{ij} is the primary input from the neurons receptive fields. L_{ij} is the secondary input of lateral connections with neighboring neurons. The interconnections M and W are the constant synaptic weight matrices for F_{ij} and L_{ij} , respectively. θ is a dynamic neuron threshold. The neuron will generate pulse when $U_{ij}(n) > \theta_{ij}(n)$. This pulse is also called one firing time. The sum of Y_{ij} in n iteration is called firing times, to represent image information, which is defined as [7]:

$$T_{ij} = T_{ij}(n-1) + Y_{ij}(n) \quad (4)$$

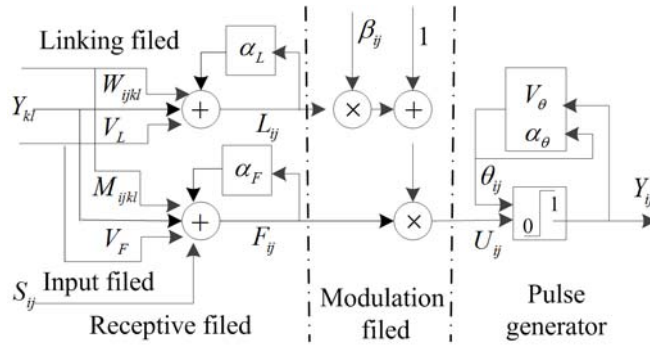


Figure 2. A PCNN neuron model

The advantage of PCNN in image fusion lies in its global coupling and pulse synchronization of neurons. In this paper, the focused regions are detected by comparing the firing times of the PCNN neurons.

3. Multi-focus Image Fusion with Sparse Feature Based PCNN

3.1. Fusion Algorithm

In this subsection, a novel algorithm of multi-focus image fusion is proposed and the fusion framework is depicted in Figure 3. For simplicity, this paper assumes that there are only two source images, namely I_A and I_B , respectively. The rationale behind the proposed algorithm applies to the fusion of more than two multi-focus images. The source images are assumed to be pre-registered and the image registration is not included in the framework. The fusion algorithm consists of the following 4 steps:

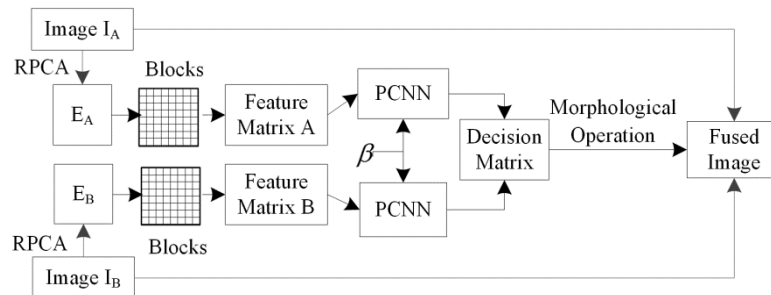


Figure 3. Block diagram of proposed multi-focus image fusion framework

Step 1: Construct data matrix D . The source images $\{I_A, I_B\}, I_A, I_B \in \mathbb{R}^{M \times N}$ is converted into column vectors $I_A^c, I_B^c \in \mathbb{R}^{MN \times 1}$, respectively. The data matrix D is defined as:

$$D = [I_A^c \ I_B^c] \tag{5}$$

Step 2: Perform RPCA decomposition on D to obtain a principal matrix $A \in \mathbb{R}^{MN \times 2}$ and a sparse matrix $E \in \mathbb{R}^{MN \times 2}$, respectively. The sparse matrix $E \in \mathbb{R}^{MN \times 2}$ is computed through inexact augmented Lagrange multipliers algorithm (IALM) of RPCA [13], which is a fast version of implementation for recovering low-rank matrices. The sparse matrix $E \in \mathbb{R}^{MN \times 2}$ is converted into matrices $E_A, E_B \in \mathbb{R}^{M \times N}$ corresponding to the source images I_A and I_B , respectively.

Step 3: Construct PCNN model with the sparse feature computed from the sparse matrices $E_A, E_B \in \mathbb{R}^{M \times N}$, respectively.

Step 4: According to the fusion rules, the focused regions of the source images are integrated to obtain the fused image.

3.2. Fusion Rules

There are two key issues [19] for the fusion rules. One is how to measure the activity level of the focused regions, which recognizes the sharpness of the source images. Figure 1 shows that the salient features of sparse matrix E agree well with the local features of the focused objects in the source images. The salient features represent the sparse features of the source images. Moreover, the advantage of PCNN in image fusion is global coupling and pulse synchronization of neurons. Thus, we use the firing times of the PCNN neurons to measure the activity level. The PCNN neurons are motivated by the sparse feature computed from the sparse matrices.

The sparse matrices E_A and E_B are divided into blocks with fixed block size, respectively. Let $E_A^{(k)}$ and $E_B^{(k)}$ denote the k th block of the sparse matrices E_A and E_B , respectively. The EOL of each block is used as the sparse feature of the source images, which can be calculated as [18]:

$$EOL = \sum_i \sum_j (E_{ii}^2 + E_{jj}^2) \quad (6)$$

$$E_{ii} + E_{jj} = -E(i-1, j-1) - 4E(i-1, j) - E(i-1, j+1) - 4E(i, j-1) + 20E(i, j) - 4E(i, j+1) - E(i+1, j-1) - 4E(i+1, j) - E(i+1, j+1) \quad (7)$$

where $E(i, j)$ indicates the value of the element at the position (i, j) in sparse matrix block.

Let $EOL_{(k)}^{E_A}$ and $EOL_{(k)}^{E_B}$ be the EOL of $E_A^{(k)}$ and $E_B^{(k)}$, respectively. The EOL of each block of the sparse matrices constructs the feature maps F_A and F_B , respectively. F_A and F_B are input to PCNN to motivate the neurons to generate pulse with Equation (3), and the firing times of the neurons are calculated with Equation (4).

The other is how to integrate the focused pixels or regions of the source images into the counterparts of the fused image. The firing times of the corresponding blocks are compared to determine which block is in focus. A decision matrix $H \in \mathbb{R}^{M \times N}$ is constructed for recording the comparison results according to the selection rule as follows:

$$H(i, j) = \begin{cases} 1 & T_k^A(n) \geq T_k^B(n) \\ 0 & \text{otherwise} \end{cases} \quad (8)$$

where '1' in H indicates the pixel (i, j) of the k th block of image I_A is in focus and '0' in H indicates the pixel (i, j) of the k th block of image I_B is in focus.

However, judging by the firing times of the PCNN neurons alone is not sufficient to detect all the focused blocks. There are thin protrusions, narrow breaks, thin gulfs and small holes in H . To overcome these disadvantages, morphological operations [20] are performed on H . Opening, denoted as $H \circ Z$, is simply erosion of H by the structure element Z , followed by dilation of the result by Z . This process can remove thin gulfs and thin protrusions. Closing, denoted as $H \bullet Z$, is dilation followed by erosion. It can join narrow breaks and thin gulfs. To correctly judge the small holes, a threshold is set to remove the holes smaller than the threshold. In this paper, the structure element Z of the proposed method is a 8×8 matrix with logical 1's and the threshold is set to 1000. Thus, the final fused image F is constructed according to the rule as follows:

$$F(i, j) = \begin{cases} I_A(i, j) & H(i, j) = 1 \\ I_B(i, j) & H(i, j) = 0 \end{cases} \quad (9)$$

where the $I_A(i, j)$ and $I_B(i, j)$ are the values of the pixels at the (i, j) in the source images I_A and I_B , respectively.

4. Experimental Results

In order to evaluate the performance of the proposed method, several experiments are performed on two pairs of multi-focus images [21, 22] vary in content and texture, as shown in Figure 4. The two pairs are grayscale images with size of 512×384 pixels and 640×480 pixels, respectively. In general, image registration should be performed before image fusion. In this paper, all the source images are assumed to have been registered. Experiments are conducted with Matlab in Windows environment on a computer with Intel Xeon X5570 and 48G memory.

For comparison, beside the proposed method, some existing multi-focus image fusion methods are also implemented on the same set of source images. These methods are discrete wavelet transform (DWT), SF (Li's method [23]), PCNN1 (Huang's method [9]), PCNN2 (Miao's method [8]), RPCA (Wan's method [15]). Due to the lack of original source code, this paper uses the Eduardo Fernandez Canga's Matlab image fusion toolbox [24] as a reference for DWT, SF. Specifically, the Daubechies wavelet function 'bi97' is used in the DWT and the decomposition level of DWT is 4. The RPCA toolbox [25] is used as the reference for RPCA decomposition. The PCNN toolbox [26] is used as a reference for PCNN1, PCNN2 and the proposed method, respectively. The parameters of PCNN1 are set as $k \times l = 13 \times 13$, $\alpha_L = 1.0$, $\alpha_\theta = 5.0$, $V_L = 0.2$, $V_\theta = 20.0$ and $N = 300$. The parameters of Miao's method are set as $k \times l = 3 \times 3$, $\alpha_L = 0.9$, $\alpha_\theta = 2.5$, $V_L = 0.2$, $V_\theta = 20.0$ and $N = 200$. The parameters of the proposed method are set as the same as that of Huang's method and the block size is 8×8 .

In order to quantitatively compare the performance of the proposed method and that of the other fusion methods mentioned above, two metrics are used to evaluate the fusion performance. They are: (i) Mutual information (MI) [27], which measures the degree of dependence of the source image and the fused image. (ii) $Q^{AB/F}$ [28], which reflects the amount of edge information transferred from the source images to the fused image. A larger value for them means a better fusion result.

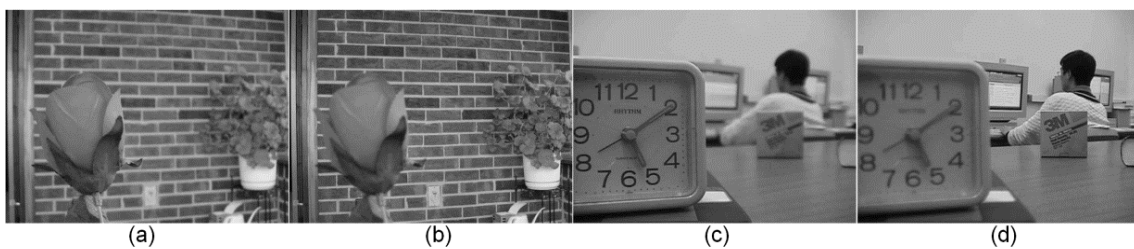


Figure 4. Multi-focus source images: (a) Near focused image 'Rose'; (b) Far focused image 'Rose'; (c) Near focused image 'Lab'; (d) Far focused image 'Lab'

4.1. Qualitative Analysis

For visual comparison, the fused images 'Rose' and 'Lab' obtained by different methods are shown in Figure 5 and Figure 6, respectively. The difference images between the far focused source image 'Lab' and their corresponding fused images obtained by different methods are shown in Figure 7.

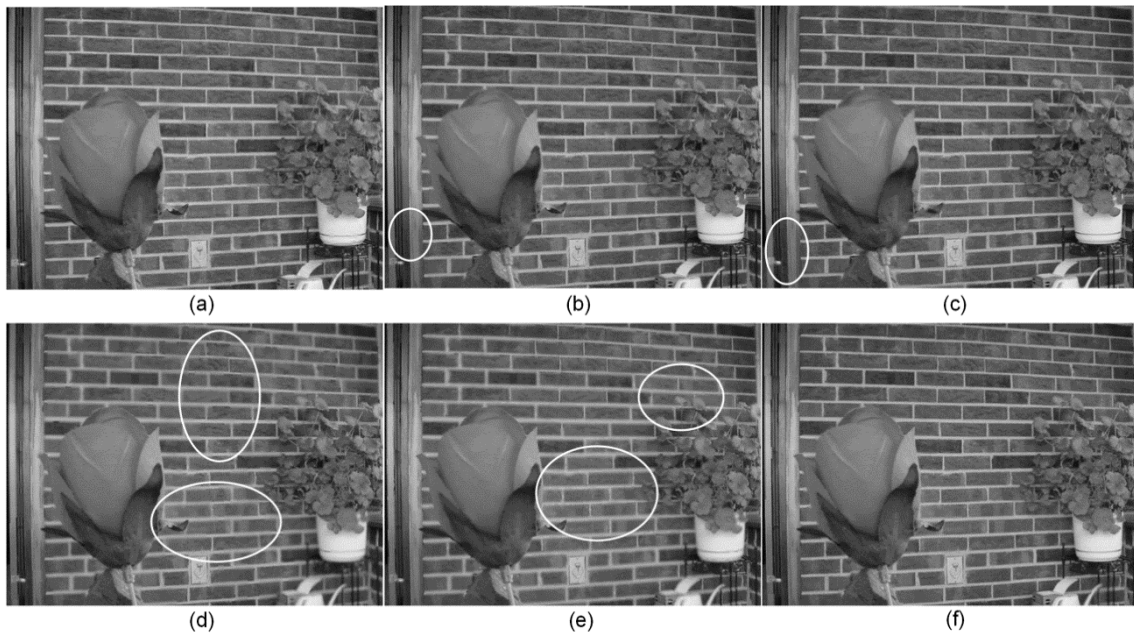


Figure 5. The fused images 'Rose' obtained by different fusion methods: (a)DWT; (b)SF; (c)RPCA; (d)PCNN1; (e)PCNN2; (f)Proposed

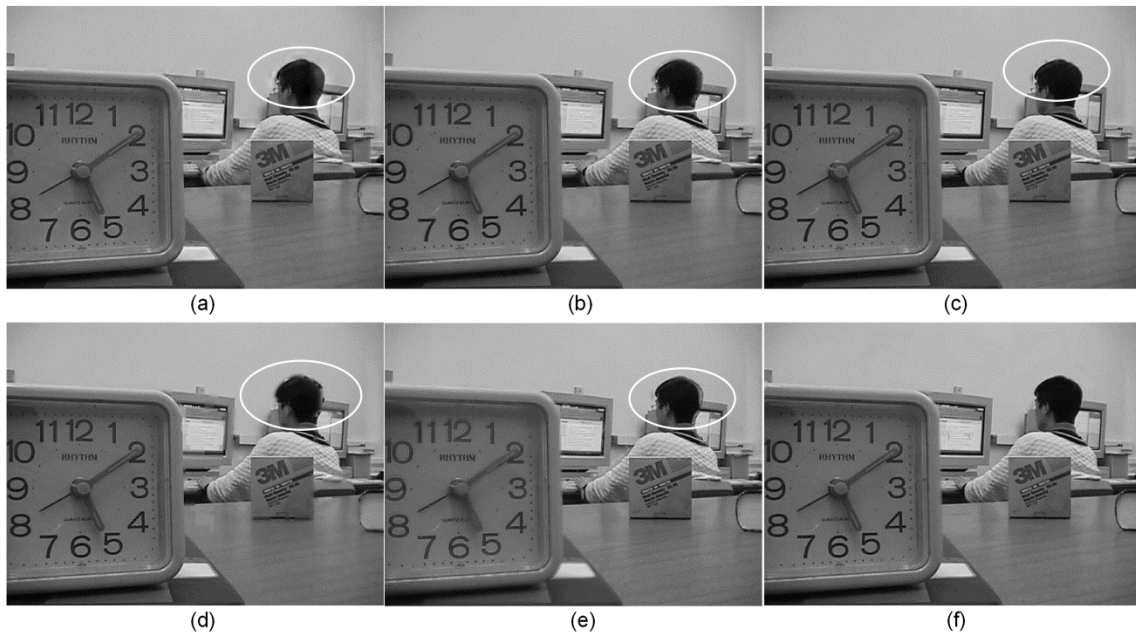


Figure 6. The fused images 'Lab' obtained by different fusion methods: (a)DWT; (b)SF; (c)RPCA; (d)PCNN1; (e)PCNN2; (f)Proposed

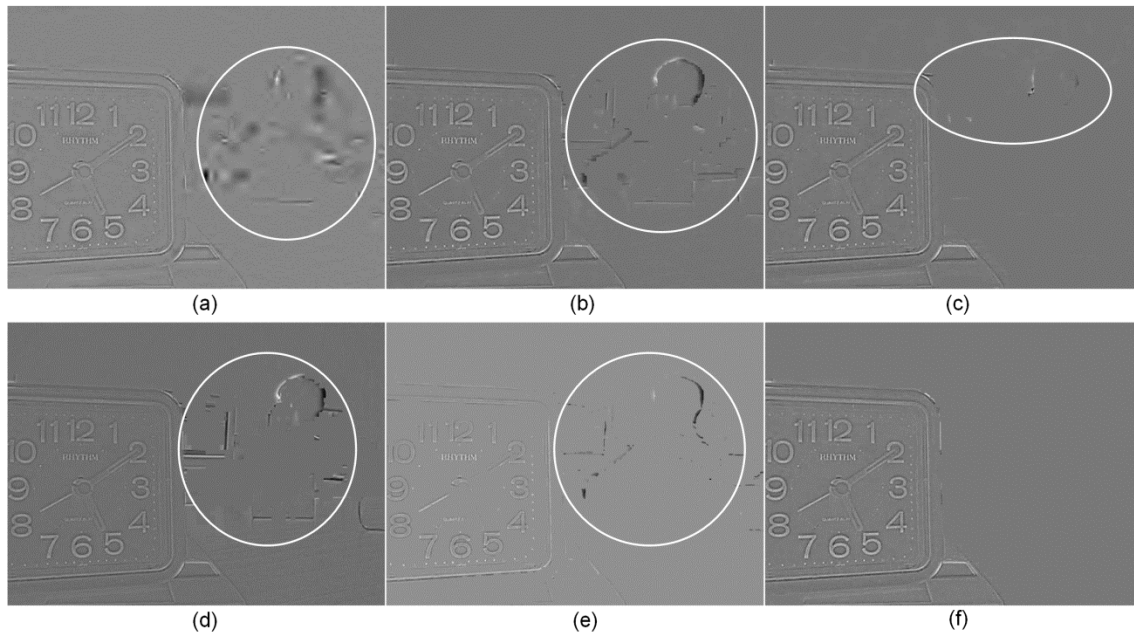


Figure 7. The difference images between the far focused source image 'Lab' and their corresponding fused images obtained by different fusion methods: (a) DWT; (b) SF; (c) RPCA; (d) PCNN1; (e) PCNN2; (f) Proposed

Inspecting the rose and the wall in Figure 5, the contrast of the fused image of DWT is worse than that of the SF, RPCA and the proposed method, and the contrast of the fused image of proposed method is better than that of the fused images of the other fusion methods mentioned above. There are some blurry regions on the wall in the fused images of PCNN1 and PCNN2, respectively. Moreover, the obvious blocking artifacts and small blurry regions appear on the door frame in the fused image of SF and RPCA, respectively. Inspecting the student and the clock in Figure 6, the student's head in the fused image of DWT shows obviously artifacts. A narrow prominent appears on the upper edge of the student's head in the fused image of RPCA. Blocking artifacts appear on the left and right edge of student's head in the fused images of PCNN1 and SF, respectively. The obvious artifact appears on the right edge of the student's head in the fused images of PCNN2. In Figure 7, mis-registration and distortion are obviously observed in the difference image of DWT. There are some obvious blocking artifacts in the difference image of SF and PCNN1, respectively. There are some obvious image residual in the right of the difference images of RPCA and PCNN2, respectively. Thus, the fused image of the proposed method achieves superior visual performance by containing all the focused contents from the source images. But it should be noted that there are also little blocking artifacts in the edge of clock in Figure 7(f). We attribute this to the fixed size of the structure element Z . To eliminate the thin protrusions, narrow breaks, thin gulfs, small holes, etc. in decision matrix H , the morphological operations are performed on decision matrix H by using the structure element Z with fixed size. The morphological operations lack adaptability for the fixed size of the structure element Z . It cannot eliminate the thin protrusions, narrow breaks, thin gulfs, small holes, etc. in decision matrix H completely.

4.2. Quantative Analysis

For quantitative comparison, the quantitative results in two quality measures are shown in Table 1. The proposed method gains highest MI [27] and $Q^{AB/F}$ [28] values compared to the other fused methods. The running times are also showed in Table 1. The proposed method requires shorter computational time than that of Wan's method. Due to the sliding window technique is applied for the detection of the focused regions, the computation of standard deviation of each sliding window in Wan's method [15] requires longer computational time than

that of the block division used in the proposed method. But the proposed method still yields longer computational cost than DWT-based fusion method and SF-based fusion method, and the matrix decomposition accounts for the majority of the computational load.

Table 1. The performance of different fusion methods

Method	Rose			Lab		
	MI	$Q^{AB/F}$	Run-time(s)	MI	$Q^{AB/F}$	Run-time(s)
DWT	4.78	0.67	0.45	6.47	0.69	0.59
SF	6.78	0.72	0.66	7.94	0.72	1.03
RPCA	7.75	0.71	39.28	8.50	0.75	60.80
PCNN1	7.45	0.64	0.51	8.86	0.71	0.55
PCNN2	6.33	0.65	20.64	8.78	0.68	32.51
Proposed	7.85	0.74	0.84	8.90	0.76	1.08

5. Conclusion

In this paper, a novel fusion method is proposed to effectively extract the focused regions and improve the quality of the fused image. The qualitative and quantitative analysis show that the proposed method achieves superior fusion results compared to some existing fusion methods and significantly improves the quality of the fused image. In the future, we will consider optimizing the proposed method to reduce the time-consuming and improving the adaptivity of the proposed method.

Acknowledgements

The work was supported by National Key Technology Science and Technique Support Program (No. 2013BAH49F03), Key Technologies R&D Program of Henan Province (No. 142102210637), the National Nature Science Foundation of China (No. 61379010), and the Natural Science Basic Research Plan in Shaanxi Province of China (No. 2012JQ1012).

References

- [1] HJ Zhao, ZW Shang, YY Tang, B Fang. Multi-focus image fusion based on the neighbor distance. *Pattern Recognition*. 2013; 46(3): 1002-1011.
- [2] ST Li, XD Kang, JW Hu, B Yang. Image matting for fusion of multi-focus images in dynamic scenes. *Information Fusion*. 2013; 14: 147-162.
- [3] H Hariharan. Extending Depth of Field via Multi-focus Fusion. *PhD Thesis*. University of Tennessee, Knoxville. 2011.
- [4] R Eckhorn, HJ Reitboeck, M Arndt, PW Dicke. Feature linking via synchronization among distributed assemblies: Simulation of results from cat cortex. *Neural Computation*. 1990; 2: 293-307.
- [5] RP Broussard, SK Rogers, ME Oxley, GL Tarr. Physiologically motivated image fusion for object detection using a pulse coupled neural network. *IEEE Transaction Neural Networks*. 1999; 10: 554-563.
- [6] JL Johnson, HS Ranganath, G Kuntimad, HJ Caulfield. Pulse coupled neural networks. *Neural Networks and Pattern Recognition*. 1998: 1-56.
- [7] ZB Wang, YD Ma, FY Cheng, LZ Yang. Review of pulse-coupled neural networks. *Image and Vision Computing*. 2010; 28(1): 5-13.
- [8] QG Miao, BS Wang. *A Novel Adaptive Multi-focus Image Fusion Algorithm Based on PCNN and Sharpness*. SPIE 2005: Sensors, and Command, Control, Communications, and Intelligence (C3I) Technologies for Homeland Security and Homeland Defense IV, Edward M. Carapezza, Editor. 2005: 704-712.
- [9] W Huang, ZL Jing. Multi-focus image fusion using pulse coupled neural network. *Pattern Recognition Letters*. 2007; 28 (9): 1123-1132.
- [10] XB Qu, JW Yan, HZ Xiao, ZQ Zhu. Image Fusion Algorithm Based on Spatial Frequency-Motivated Pulse Coupled Neural Networks in Nonsampled Contourlet Transform Domain. *Acta Automatica Sinica*. 2008; 34(2): 1508-1514.
- [11] ZB Wang, YD Ma, J Gu. Multi-focus image fusion using PCNN. *Pattern Recognition: The Journal of*

- the Pattern Recognition Society*. 2010; 43(6): 2003-2016.
- [12] P Geng, X Zheng, ZG Zhang, YJ Shi, SQ Yan. Multifocus Image Fusion with PCNN in Shearlet Domain. *Research Journal of Applied Sciences, Engineering and Technology*. 2012; 4(15): 2283-2290.
- [13] E Candes, X Li, Y Ma, J Wright. Robust principal component analysis?. *Journal of the ACM*. 2011; 58(3): 1-37.
- [14] W Zou, K Kpalma, Z Liu, and et al. *Segmentation Driven Low-rank Matrix Recovery for Saliency Detection*. 24th British Machine Vision Conference (BMVC). Bristol. 2013: 1-13.
- [15] T Wan, CC Zhub, ZC Qin. Multifocus Image Fusion Based on Robust Principal Component Analysis. *Pattern Recognition Letters*. 2013; 34(9): 1001-1008.
- [16] J Wright, A Ganesh, S Rao, Y Ma. *Robust principal component analysis: Exact recovery of corrupted low-rank matrices via convex optimization*. Proceedings of Advances in neural information processing systems. 2009: 2080-2088.
- [17] Z Lin, M Chen, L Wu, Y Ma. *The augmented Lagrange multiplier method for exact recovery of corrupted low-rank matrices*. UIUC Technical Report UILU-ENG-09-2215. 2009.
- [18] W Huang, Z Jing. Evaluation of focus measures in multi-focus image fusion. *Pattern Recognition Letters*. 2007; 28(4): 493-500.
- [19] Y Jiang, M Wang. Image fusion with morphological component analysis. *Information Fusion*. 2014; 18: 107-118.
- [20] B Yang, ST Li. Multi-focus image fusion based on spatial frequency and morphological operators. *Chinese Optics Letters*. 2007; 5(8): 452-453.
- [21] <http://www.ece.lehigh.edu/spcrl>. 2005.
- [22] <http://www.imgfsr.com/sitebuilder/images>. 2009.
- [23] S Li, JT Kwok, Y Wang. Combination of images with diverse focuses using the spatial frequency. *Information fusion*. 2001; 2(3): 169-176.
- [24] Image fusion toolbox: <http://www.imagefusion.org/>.
- [25] RPCA toolbox: http://perception.csl.illinois.edu/matrix-rank/sample_code.html.
- [26] PCNN toolbox: http://quxiaobo.go.8866.org/project/PCNN/PCNN_toolbox.rar.
- [27] DJC MacKay. *Information theory, inference and learning algorithms*. Cambridge university press. 2003.
- [28] CS Xydeas, V Petrovic. Objective image fusion performance measure. *Electronics Letters*. 2000; 36: 308-309.